X-ray absorption spectroscopy studies of local structure and electronic properties of Na_xSi_{136} $(0<x<24)$ clathrates

Andrew D. Ritchie,[1,2] Mark A. MacDonald,[1,2] Peng Zhang,[1,2] Mary Anne White,[1,2,3,*] Matt Beekman,[4] Jan Gryko,[5] and George S. Nolas[4]

[1]*Department of Chemistry, Dalhousie University, Halifax, Nova Scotia, Canada B3H 4J3*

[2]*Institute for Research in Materials, Dalhousie University, Halifax, Nova Scotia, Canada B3H 1W5*

[3]*Department of Physics and Atmospheric Science, Dalhousie University, Halifax, Nova Scotia, Canada B3H 3J5*

[4]*Department of Physics, University of South Florida, 4202 E. Fowler Ave., Tampa, Florida 33620, USA*

[5]*Department of Physical and Earth Sciences, Jacksonville State University, Jacksonville, Alabama 36265, USA*

(Received 20 April 2010; revised manuscript received 16 September 2010; published 19 October 2010)

We have probed both the local structure and the electronic properties of Na-containing type II Si clathrates by x-ray absorption spectroscopy. The near-edge region of the spectrum is particularly sensitive to the local structure surrounding the Na atom. Through experimental investigations of a series of eight samples with general formula Na_xSi_{136}, with x ranging from ~0 to 21.5, and simulation of extended x-ray absorption fine structure (EXAFS) and x-ray absorption near-edge structure spectra (XANES), we find that Na is primarily in the larger Si_{28} cages at low loadings, and loss of the Na relative to full cage occupancy occurs preferentially from the smaller Si_{20} cages. Our EXAFS results also show that Na is dynamically disordered in the Si_{28} cages but less disordered at higher Na loadings. Local-orbital density of states calculations indicate that the Na in the Si_{20} cage has a charge of $0.7e^-$ while Na in the Si_{28} cages has a slightly higher (loading-dependent) charge ($0.72e^-$ to $0.8e^-$).

DOI: 10.1103/PhysRevB.82.155207 PACS number(s): 78.70.Dm

I. INTRODUCTION

Known since the mid 1960s,[1] intermetallic clathrates have received considerable attention in the literature in recent years.[2] Renewed interest has been related to their potential role in development of more efficient thermoelectric materials, using the concept of a phonon glass electron crystal (PGEC). This is an idealized material that combines electrical transport characteristic of a single-crystal semiconductor with glasslike thermal transport,[3] based on phonon disrupting rattlers.[4] The PGEC approach has proven a practical route to maximizing the efficiency of thermoelectrics by tailoring the most influential contributing properties.[5,6]

Analogous to the clathrate hydrate structure,[1] semiconductor clathrates are comprised of a continuous network of face-sharing polyhedra encapsulating various guest species.[7–9] Whereas the framework of a clathrate hydrate can act as a storage medium for such compounds as methane gas and CO_2, in semiconductor clathrates the framework provides a continuous conductive pathway for electricity (electron crystal) while the encaged guest atoms, often referred to as "rattlers," provide dynamic disorder that hinders phonon propagation and thus reduces thermal conductivity (phonon glass).

As for the clathrate hydrates, intermetallic clathrates come in a variety of "types."[5,10–12] However, by far the most common are types I and II which are also known structures for clathrate hydrates.[1] Type I is comprised of six tetrakaidecahedra (24-atom cages) for every two dodecahedra (20-atom cages)[13] while the type II clathrate is made up of eight hexakaidecahedra (28-atom cages) with 16 dodecahedra.[14]

Semiconductor clathrates offer an opportunity to better understand the complex structure-property relationships that define the suitability of a material for thermoelectric applications. Type I clathrates are typically stoichiometric crystalline solids that can accommodate a wide variety of guest atoms. For example, Na_8Si_{46} exhibits glasslike lattice thermal conductivity[15,16] due to enhanced low-temperature anharmonicity associated with motions of the guests in the cages.[17] Both the host and the guest composition can be changed,[18] and varying the elements incorporated as guests has lead to the conclusion that small, heavy rattler atoms produce the most dramatic decreases in lattice thermal conductivity.[19] In addition to varying guest identity, the guest loadings are tunable in type II clathrates. Altering the guest concentration of type II clathrates can be accomplished by removing some of the guest atoms from a fully occupied type II structure.[20,21] This ability to remove guest atoms has led to the production of nearly empty clathrate samples with negligible guest concentrations and the further discovery that the clathrate framework itself contributes significantly to lower the lattice thermal conductivity of these structures when compared to more compact structures,[22,23] as also found for an organic clathrate.[24] However, the details and mechanisms of how the Na atoms are removed from the two different cages remain intriguing open questions.

The structures of many clathrate systems have been studied by x-ray diffraction (XRD).[18,25] These studies have provided detailed information about the structure for the stoichiometric type I clathrates. In type II structures, the composition, i.e., guest content, is tunable, adding complexity to the interpretation of experimental data. Specifically, there have been conflicting findings with regard to the occupancies of the two different polyhedral cages that compose the type II structures. Powder x-ray diffraction studies have suggested that the smaller Si_{20} polyhedra are the first to lose their Na guests, and the larger Si_{28} cages are evacuated only after all of the small-cage Na atoms have been removed.[26–28]

This has been further supported by theoretical studies that attribute the preferential loss from the small cages to a decreased stability stemming from stronger Na-Si repulsion in the smaller Si_{20} cages.[29] One interpretation of NMR data suggested that there is a preferential loss from the Si_{20} cages[30] while another suggested loss occurs preferentially from Si_{28} cages.[31] Understanding cage occupation is important because as x approaches 9, Na_xSi_{136} transitions from metallic to insulating behavior.[28] Some authors have suggested that the displacement of the Na atoms from the center of the larger Si_{28} cage leads to a Peierls-type distortion related to the preferential occupation of the Si_{28} cages.[32] However, the precise location of Na within the larger Si_{28} cages has been the subject of some controversy with both experiments and calculations indicating a range of displacements from the center of those cages.[26,29,32,33] In the present study, we use x-ray absorption spectroscopy (XAS) to examine the structural details of a series of eight Na-containing Si clathrates of the general formula Na_xSi_{136}, where x was varied from ~0 to 21.5 in order to provide further insight into the location of the Na atoms. This information is important in relation to the physical properties of these materials.

The very bright, tunable x-rays made available by synchrotron light sources provide an opportunity for detailed XAS studies to probe the interactions of the Na and Si atoms. XAS is particularly suitable here to probe the structural and electronic properties from both the Na and the Si perspectives. Using both spectroscopic calculations and samples that include a wide range of Na rattler concentrations ($0 < x < 21.5$), we have systematically probed local structure and electronic properties of Na-containing type II Si clathrates.

II. METHODS

Samples were prepared at the University of South Florida by the method of thermal decomposition of Na_4Si_4, as described by Cros *et al.*[34] First, the precursor Na_4Si_4 was synthesized by heating a stoichiometric mixture of high-purity Si powder and high-purity Na to 650 °C for 36 h in a sealed stainless-steel container, under an ultrahigh-purity nitrogen atmosphere. The Na_4Si_4 precursor was then decomposed by rapid heating under dynamic vacuum (10^{-6} Torr) to 360 °C to produce a nearly full sample ($23 < x < 24$). The Na content (determined by Rietveld refinement) for the different compositions listed in Table I was controlled by further heating under vacuum. The preparation of the elemental Si_{136} clathrate sample ($x \to 0$) is described in detail elsewhere.[35]

TABLE I. Sample compositions along with known impurity phases, obtained from the preparation method described in the text.

x	Estimated Na_8Si_{46} fraction (mass %)	Estimated α-Si fraction (mass %)
0 (Ref. 22)	0	<4
1.3	3	1
5.5	3	<1
6.5	3	<1
7.2	3	<1
8.8	5	<1
14.1	3	<1
21.5	2	<1

The composition of the samples was determined by Rietveld analysis of powder x-ray diffraction data, with the aid of the GSAS (Ref. 36) and EXPGUI (Ref. 37) software. The relative intensities of the majority of the Na_xSi_{136} reflections are very sensitive to the Na content in the two distinct cages. In this way, the cage occupancies and therefore composition can be determined. Our Rietveld analysis indicates that for $x < 8$, Na shows strong preferential occupation of the larger Si_{28} cage, and for $x > 8$ the Si_{20} cages become substantially occupied. This is in agreement with previous powder x-ray diffraction studies.[1,26–28]

Si K-edge and Na K-edge absorption spectra were gathered at room temperature at the high-resolution spherical grating monochromator (SGM) beamline at the Canadian Light Source in Saskatoon. Although the Na_xSi_{136} clathrates are very stable toward air and moisture, samples were stored under nitrogen until immediately before measurements were taken in order to limit surface exposure of the fine powders to oxygen. The powder samples were mounted on carbon tape on a stainless-steel disk. Both total-electron (TEY) and fluorescent yields (FLY) were measured. Resolution at the Si K-edge is approximately 0.2 eV on this beamline. As an example of the methodology, Fig. 1 presents the total electron yield for both the sodium signal and the silicon signal from the $Na_{21.5}Si_{136}$ sample.

Data refinement followed a standard nonlinear least-squares method in R space using the WINXAS software package. Fourier transformation of $\chi(k)$ was conducted for k of 2.4 to 7 Å^{-1} while data refinement was performed in R space in the region from 2 to 4.2 Å. This was done for both $\chi(k)^*k$

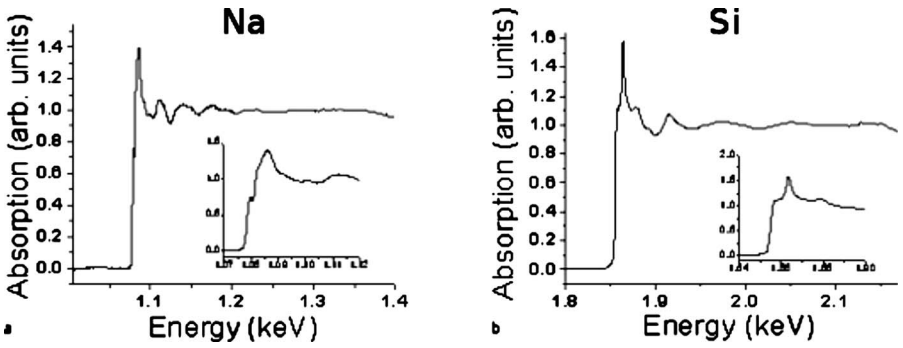

FIG. 1. X-ray absorption spectroscopic raw data for $Na_{21.5}Si_{136}$ at (a) the Na K edge and (b) the Si K edge. Near-edge regions are presented in more detail as insets.

and $\chi(k)^*k^2$, yielding similar results in each case.

In all cases, the amplitude reduction factor, S_o^2, was fixed at a value of 0.6 based on the sample with the highest Na concentration ($x=21.5$) as per previous methods.[38] Theoretical Na-Si coordination numbers were based on sodium occupancy in the Si_{20} and Si_{28} cages obtained from Rietveld refinement of powder x-ray diffraction patterns and fixed during refinement. All other fitting parameters $[R(\text{avg}), \sigma^2, E_o]$ were extracted from the experimental data.

The FEFF8 software package[39] was used to simulate spectra and to carry out local (orbital) density of states (LDOS) calculations, based on models built using the CRYSTALMAKER™ software. A variety of potentially important parameters that were observed to change with Na content such as lattice constant, Na content, and guest position were varied in order to determine their impact on simulated spectra. Resulting spectra were then compared to experiment and models were revised to optimize agreement between experiment and simulation. Varying Na content was found to have no observable effect on the outcome of simulations even in combination with other significant factors, namely position within the Si_{28} cages. As such, simulations were based on models that included only relevant, absorbing, Na atoms. The position of the Na within the large cages was found to have the most significant impact on simulated spectra and thus was optimized as discussed below.

III. RESULTS AND DISCUSSION

A. Na *K*-edge EXAFS and simulation

The Na *K*-edge extended x-ray absorption fine structure (EXAFS) spectra are very sensitive to Na-Si interactions, and this information can be used in a semiquantitative fashion to discern the relative proportions of Na in the larger Si_{28} cages, compared with Na in the smaller Si_{20} cages.

Figure 2(a) shows the weighted-average combinations of calculated Na *K*-edge EXAFS spectra. Simulations used for this averaging included the Si framework (treated as fully occupied on all sites, in accord with our Rietveld analysis results for all specimens studied here as given in the supplementary information[40] using the same data collection and structural refinement strategy as in our earlier work[41]) and only the interactions of Na atoms with their local environment (neighboring Si) were included. That is, Na atoms were treated as independently absorbing in the EXAFS simulations since Na-Na interactions were found to have no observable impact on the EXAFS spectra produced, as one would expect given the long Na-Na distances. As such, the simulated spectra in Fig. 2(a) illustrate the shift in EXAFS from one extreme, completely Na in Si_{28} character, to the other, completely Na in Si_{20} character, and do not account for any differences due to changing overall framework occupancy. At the extremes of the relative occupancy range, where one Na environment is significantly in the majority, the correlation between the peaks and the Na environment can be seen clearly. By comparing the simulated EXAFS spectra in which Na is either fully occupying the Si_{20} cages or the Si_{28} cages [top and bottom of Fig. 2(a), respectively], it is evident that for Na in Si_{28} cages that the EXAFS oscillation intensity

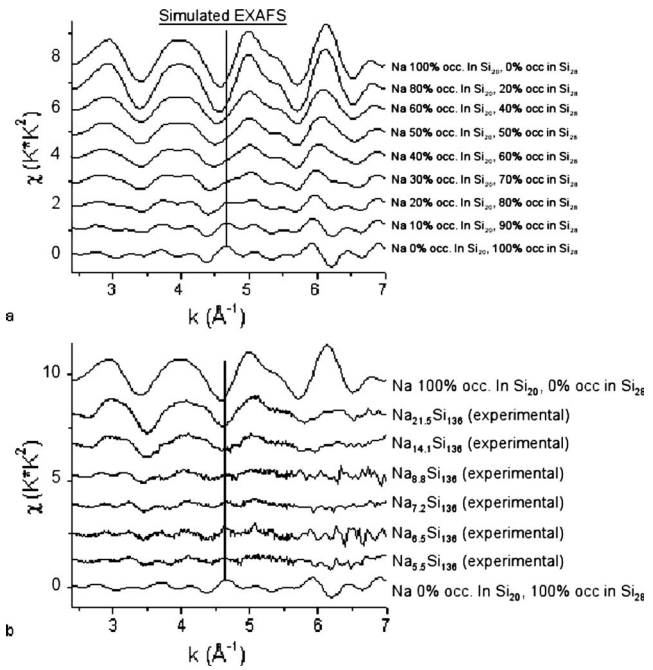

FIG. 2. (a) Simulated and (b) both experimental and simulated Na *K*-edge EXAFS spectra of several representative samples of Na_xSi_{136}. For the simulation, the Si framework is considered to be the same in all cases, the displacement of Na off the center of the Si_{28} cages is 0.5 Å for all simulations and the percent occupancy of the Na in the Si_{20} cages and Na in the Si_{28} cages varies as indicated. The vertical line marks the position of the dominant oscillation for Na in the larger (Si_{28}) cages.

is much lower and the oscillation frequency is higher than that for Na in Si_{20} cages. This correlates well with the experimental findings [Fig. 2(b)] for low Na loading ($Na_{5.5}Si_{136}$) and high Na loading ($Na_{21.5}Si_{136}$), which are dominated by Na in Si_{28} cages and in Si_{20} cages, respectively, as discussed further below. The intermediate simulations in Fig. 2(a) are based on appropriate weightings of the simulations based on full occupation of the Si_{20} cages and full occupation of the Si_{28} cage, such that, for example, "Na 80% occupancy in Si_{20}, 20% occupancy in Si_{28}" refers to simulation of composition of $Na_{14.4}Si_{136}$, in which there are 12.8 (out of a possible 16) Na atoms in the Si_{20} cages, and 1.6 (out of a possible 8) Na atoms in the Si_{28} cages.

According to theory,[42] EXAFS intensity $\chi(k)$ can be expressed as

$$\chi(k) = \sum_j \frac{N_j S_0^2 F_j(k)}{kR_j^2} \cdot e^{(-2k^2\sigma^2)} \cdot e^{(-2R_j/\lambda)} \sin[2kR_j + \delta_j(k)], \tag{1}$$

where $F(k)$ is the backscattering amplitude from each of the N_j neighboring atoms of the jth type at an interatomic distance R_j, with a Debye-Waller factor of σ_j to account for thermal vibrations (assumed to be harmonic) and static disorder (assuming Gaussian pair distribution). The quantity $\delta(k)$ is the total phase shift experienced by the photoelectron, S_0^2 is the amplitude reduction factor, and λ is the photoelectron mean-free path. The average interatomic distance be-

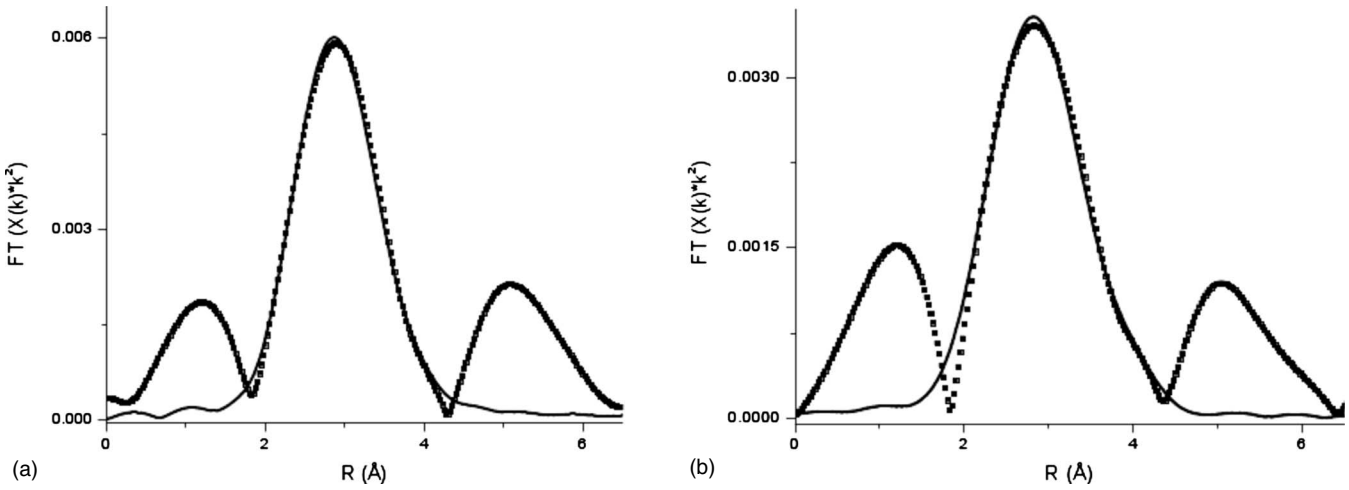

FIG. 3. EXAFS refinement. Experimental data (dots) and the fit (line) are presented for (a) $Na_{21.5}Si_{136}$ and (b) $Na_{14.1}Si_{136}$.

tween the Na and neighboring Si atoms is shorter for the Si_{20} cages than for the Si_{28} cages. From the form of Eq. (1), especially $\chi(k) \sim R_j^{-2} \exp(-R_j)$, Na in the Si_{20} cage generates a significantly greater EXAFS intensity, $\chi(k)$. Equation (1) shows that the EXAFS oscillation frequency is mainly determined by the term $\sin[2kR_j + \delta_j(k)]$, and therefore a longer Na-Si interatomic distance corresponds to a higher oscillation frequency in k space. Therefore, comparison of the intensity and oscillation frequency of the EXAFS results can provide information concerning the Na occupancy in the different Si cages. In particular, the EXAFS oscillation band at ~ 4.7 Å^{-1}, which is prominent for Na in Si_{28} cages, diminishes rapidly as the occupancy of Na in the smaller Si_{20} cages increases [Fig. 2(a)]. By comparing this, the most prominent observable feature for Na in the Si_{28} cages, indicated by the vertical lines in Figs. 2(a) and 2(b), with simulation, we find that the fine-structure features for Na in Si_{20} cages become dominant when more than $\sim 30\%$ of the total Na content is in the Si_{20} cages. Therefore, the intensity of the 4.7 Å^{-1} oscillation band can be used to estimate the concentration of Na in Si_{28} when visible (i.e., $>70\%$ of Na in Si_{28}). When the band at 4.7 Å^{-1} disappears, the Na occupancy in Si_{28} is $<70\%$. From the experimental data in Fig. 2(b), it can be seen that this threshold occurs in Na_xSi_{136} for $x \sim 8.8$, i.e., Na_xSi_{136} for $x > 8.8$ is dominantly Na in Si_{20} cages, and for $x < 8.8$ is dominantly Na in the larger Si_{28} cages.

Figure 2(b) shows that the experimental EXAFS oscillating pattern of the highest Na-loading sample, $Na_{21.5}Si_{136}$, is essentially identical to the simulated spectrum for Na in the Si_{20} cages only. This observation is consistent with nearly full Na loading, since the Si_{136} framework has twice as many Si_{20} cages as Si_{28} cages, and the EXAFS features for Na in Si_{20} are more intense than for Na in Si_{28}, as discussed above. Although experimental EXAFS spectra for low-Na-content samples ($Na_{6.5}Si_{136}$ and $Na_{7.2}Si_{136}$) in the high-k region ($k > 6$ Å^{-1}) are rather noisy, the six oscillations in the low-k region are distinct, and very similar to those of the spectrum simulated for Na in Si_{28} cages. The oscillation bands at ~ 4.7 Å^{-1} (characteristic for Na in Si_{28}) for the two lowest Na-content samples are of considerable intensity, indicating that the Na in Si_{28} cages dominates in these two samples. A close comparison with the simulated EXAFS in Fig. 2(a) leads to an estimation of 80–90 % occupancy of Na in Si_{28} cages in $Na_{5.5}Si_{136}$ and $Na_{6.5}Si_{136}$ and 70–80 % of Na in the Si_{28} cages in $Na_{7.2}Si_{136}$ and $Na_{8.8}Si_{136}$. Thus, over the loading range from $x=8.8$ to $x=5.5$ for Na_xSi_{136}, the Na occupancy in Si_{28} cages estimated from EXAFS drops from $\sim 80\%$ to $\sim 60\%$ while the occupancy of Na in the Si_{20} cages drops from $\sim 15\%$ to $\sim 5\%$. Therefore, the Na K-edge EXAFS results show that at low loadings, most of the Na is in the Si_{28} cages, and loss of Na during preparation occurs preferentially from the smaller Si_{20} cages. This result is in agreement with our Rietveld analysis of powder x-ray diffraction data for these specimens.

From Fig. 3, it can be seen that data refinement produced a good fit for the EXAFS region of the $Na_{21.5}Si_{136}$ and $Na_{14.1}Si_{136}$ spectra. Table II presents the quantitative data obtained from this procedure. Average bond distances, R(avg), obtained from EXAFS refinement are in good agreement with those obtained from x-ray diffraction studies.[41] Na in the Si_{20} cages appears to have a consistent Debye-Waller factor across the two refinable spectra while those of the Na in the Si_{28} cages increase with decreasing Na content. This trend is qualitatively continued to the $x=8.8$ sample. However, the XAS data become noisier with decreasing Na content and quantitative conclusions have not been possible for $x < 14.1$. These values, while large compared to those typical of crystalline materials, are in line with the dynamical disorder associated with the guests in clathrate structures. The smaller Debye-Waller factor for $x=21.5$ compared with $x=14.1$ indicates less dynamical disorder of the Na atoms in the Si_{28} cages with increased loading. This refinement thus supports the hypothesis that dynamic disorder and displacement off the center of the Si_{28} cages increase with decreasing Na content.

B. Experimental Na *K*-edge XANES spectra and FEFF simulations

1. Off-center displacement of Na in the larger cages

The Na atom is a tight fit in the smaller Si_{20} cage but the larger Si_{28} cage has sufficient room for the Na atom to move

TABLE II. Quantitative results obtained from EXAFS refinement. The coordination number (CN) was obtained from x-ray diffraction studies and fixed for the refinement while the remaining variables were determined through the fitting procedure. E_o is an empirical parameter that was constrained within ±5 eV during refinement.

x	Path	CN	R(avg) (Å)	R(avg) XRD (Å)	ΔR (%)	σ^2 (Å^2)	E_o (eV)
21.5	Na-Si_{20}	12.7	3.278(2)	3.307	0.9	0.0230(2)	−0.12(4)
	Na-Si_{28}	10.3	4.08(1)	3.979	2.5	0.0377(8)	0.4(1)
14.1	Na-Si_{20}	8.7	3.227(3)	3.318	2.7	0.0271(2)	−2.5(2)
	Na-Si_{28}	15.9	4.06(1)	3.969	2.3	0.0565(9)	0.34(7)

off-center[32] as well as dynamically rattle.[43] We have explored the effect of the displacement of the Na atom from the center of the Si_{28} cage by simulation of the Na K-edge x-ray absorption near-edge structure (XANES) spectra. The results are shown in Fig. 4. The most direct comparison with experiment is for the lowest loading ($Na_{1.3}Si_{136}$) because virtually all Na atoms are in the larger Si_{28} cages. This comparison shows that simulated spectra for displacements of the Na atoms in the Si_{28} cages ranging from 0.4 to 0.6 Å most closely resemble those obtained from experiment. A previous study concluded that NMR results are consistent with *either* the Na atoms in a static position at the center of the Si_{28} cage, *or* the Na are dynamically disordered but symmetric about the center of the Si_{28} cage (but not statically disordered off center).[31] Our XANES results and also our powder XRD refinements[44] both indicate displacements of the Na in the Si_{28} cages of 0.5 Å, uncertain to within ±0.1 Å. Therefore, taking this together with the NMR results,[31] we can conclude that Na is dynamically disordered in the Si_{28} cages. Unfortunately, from the peak shapes and peak positions in the XANES simulations we were not able to confirm small changes in displacement with loading, as we see from the powder XRD refinement (~0.4 Å at higher Na content to ~0.6 Å at lower Na content).[41,44] Therefore, the median off-center displacement, 0.5 Å, was used for Na in the Si_{28} cages in all further simulations. This displacement also was used for the Na in the Si_{28} cages in the EXAFS spectra discussed above. Earlier EXAFS studies of the same system have shown similar but slightly larger displacement of the Na from the center of the Si_{28} cages (0.9 ± 0.2 Å) (Refs. 32 and 45) although local-density approximation calculations indicate a displacement of 0.5 Å.[33] Although regular fitting of the data in the EXAFS region gives more accurate results regarding the average bond distances for an absorbing atom, it does not indicate the atom's position relative to the origin of the unit cell or its relative position within a structure such as the Si cages. This means that a nonroutine fitting method must be used to determine Na displacement from the EXAFS region, increasing the associated error (the uncertainty for regular fitting is ~0.02 Å compared to ~0.2 Å for the nonroutine fitting discussed here). While the XANES method used herein relies on calculations for Na displacement determination, and is therefore also indirect, given the high-quality powder XRD data and close agreement between the two determinations, the current method appears to be quite reliable. In addition, by determining the displacement using a sample in which the majority, if not all, of the Na atoms reside in the relevant Si_{28} cages, the determination is further simplified and representative of the physical situation being examined.

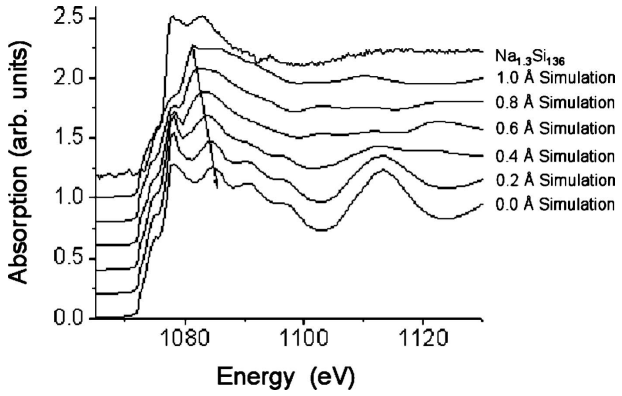

FIG. 4. By comparing simulated Na XANES spectra to the experimental $Na_{1.3}Si_{136}$ spectrum, the magnitude of the displacement of the Na atom from the center of the Si_{28} cage was estimated. In the simulations, the Na atom displacement from the center of the cage along the cube diagonal was varied from 0 to 1 Å, as indicated. The arrow shows the systematic shift in one peak with displacement. Comparison of the resulting simulated XANES spectra to the experimental spectrum for $Na_{1.3}Si_{136}$, a sample containing only Na in the large Si_{28} cages, indicates that best agreement at that loading is obtained when the displacement is ~0.5 Å.

Note that XANES simulations run using models in which all cages were occupied by Na atoms were negligibly different from simulations in which only the scattering Na atom was included. In other words, the simulated spectra show little change with Na loading, and depend only on the location of the absorbing atom (whether it is in a Si_{20} or in a Si_{28} cage). This result indicates that XANES spectral features are more dependent on the multitude of Si nearest neighbors than the relatively sparse Na neighbors, as one might expect.

2. Cage occupancy from comparison with experimental XANES data

Figure 5 shows the experimental and simulated Na K-edge XANES spectra for the full range of Na contents. In the experimental data [Fig. 5(a)], the lowest Na-content samples, $x \to 0$ and $x = 1.3$, show a doublet (indicated by two arrows) immediately following the absorption edge. Simula-

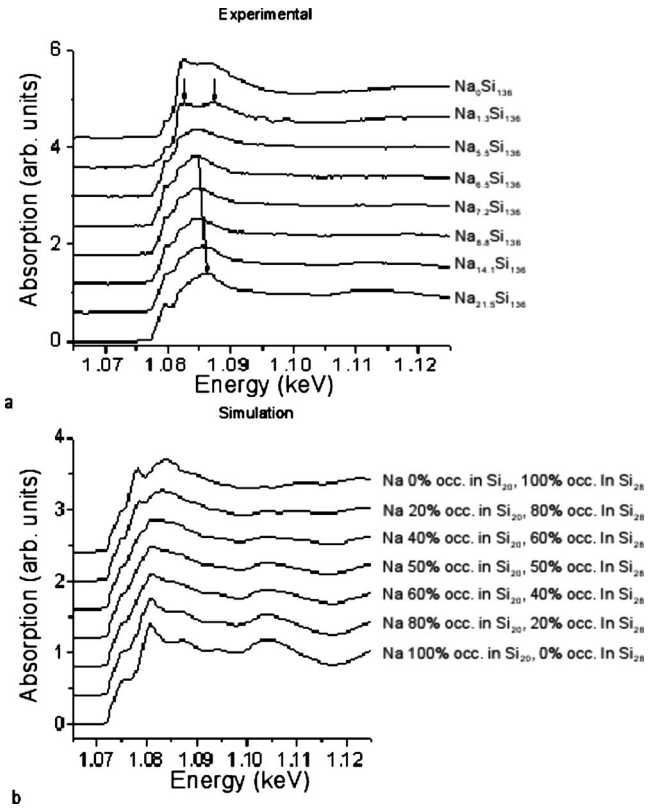

FIG. 5. Effect of distribution of Na in Na_xSi_{136} in the Si_{28} and Si_{20} cages. (a) Experimental XANES results and (b) simulated XANES spectra with the occupancy of Na in the larger Si_{28} and smaller Si_{20} cages varying as indicated. In (a), the upper pair of arrows indicates features associated with Na in Si_{28}. The lower arrow shows how the most intense feature shifts with increased Na loading.

tions of Na in the Si_{28} cages, Fig. 5(b), show the same features at the same energies as observed experimentally for the low-Na content samples, whereas simulations of Na in the Si_{20} cages produced a peak intermediate to the two components of the doublet. Therefore, the observation of a doublet with no intermediate peak is indicative that Na is present only in the Si_{28} cages.

Inspection of the experimental spectra in Fig. 5(a) reveals that the doublet (characteristic for Na in the Si_{28} cages) diminishes rapidly as x increases, and is accompanied by the appearance of a peak at an intermediate energy, 1.085 keV from the experimental XANES spectra. Comparison with the simulations [Fig. 5(b)] shows that this intermediate peak is characteristic of Na in the Si_{20} cages. These observations suggest that the XANES spectral contribution of Na in the Si_{20} cages of Na_xSi_{136} increases as x increases from 1.3 to 5.5 and above. However, it is known that the x-ray near-edge absorption cross section is sensitive to interatomic bond distance such that a shorter bond distance corresponds to a greater cross section.[46] Unlike EXAFS, our simulation of XANES spectra only generates normalized spectra (i.e., the absorption cross section is not considered). Consequently, the Si_{28}/Si_{20} cage occupancy cannot be quantitatively evaluated by comparing the results in Figs. 5(a) and 5(b). Nevertheless, based on the results of cage occupancy obtained from the EXAFS data discussed above, it is likely that a small increase in the concentration of Na in the Si_{20} cages can result in a significant change in the XANES spectra. In other words, these findings indicate that the Na K-edge XANES spectrum is more sensitive to the change in local structure of the samples than EXAFS is, and the presence of a doublet peak in the XANES spectrum indicates that Na in the larger Si_{28} cages is responsible for a significant majority of the x-ray absorption signal.

Figure 5(a) shows that for $x>6.5$, a shift of the most intense XANES peak to higher energy with increasing Na content is observed experimentally. This broad peak contains character from both Na in Si_{28} and Na in Si_{20}. Simulations presented in Fig. 4 suggest that the peak position in the near-edge region migrates toward higher energies as the Na guest moves toward the center of the Si_{28} cage. When Na in the Si_{28} cage is modeled as off-center at the 32e crystallographic site, our Rietveld refinements indicate that the magnitude of the off-center displacement decreases with increasing Na content. We tentatively attribute the observed peak migration to higher energies to the changing Na position within the Si_{28} cages resulting from changing Na content, as per the observations from Rietveld analysis.

3. Calculation of LDOS

LDOS calculations for Na presented in Fig. 6 show that the absorption edge is dominated by p-orbital contributions as expected. These calculations also indicate that Na in the Si_{20} cage has a charge of $+0.7e^-$ and Na in the Si_{28} cage has a slightly higher charge, $+0.72e^-$ at high loading and $\sim +0.8e^-$ at lower loadings. Such a small change in charge transfer, especially when averaged over Na in both the Si_{20} and Si_{28} cages, is too subtle under the conditions of this study to be detectable by a K-edge shift. While these values cannot be supported quantitatively by our experimental syn-

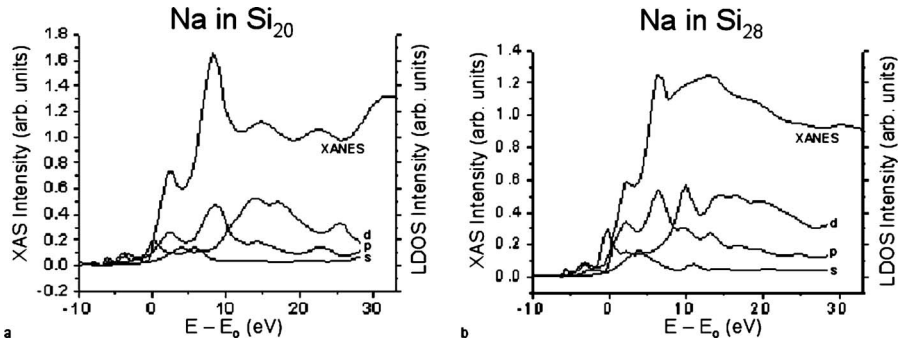

FIG. 6. Calculated LDOS and simulated XANES for Na in Na_xSi_{136}, in (a) Si_{20} cages, and (b) in Si_{28} cages. The major peaks for Na in Si_{20} are due to the excitation of a core electron to the HOMO, p-orbital, and the doublet for Na in Si_{28} appears to be due to excitation into the unoccupied p and d orbitals.

TABLE III. Calculated charge transfer for Na atoms in the Si_{28} cage of Na_xSi_{136}, as a function of displacement of Na from the center of the cage.

Displacement off-center (Å)	Calculated charge transfer (e^-)
0	0.862
0.2	0.865
0.4	0.847
0.6	0.808
0.8	0.735
1.0	0.646

chrotron studies, they are in agreement with the redshift observed relative to a Si wafer standard. This is further supported by earlier Compton scattering studies for the closely related type I system which indicated a charge of $+0.69e^-$ for Na in the Si_{20} cages and $+0.78e^-$ for Na in the Si_{24} cages.[47] Given the observed Si redshift, the similar nature of the two structures, and that density-functional theory studies of both the type I and type II systems have indicated increased charge transfer with cage size,[29] it is reasonable that both structures follow similar trends.

As discussed above, it is likely that Na is displaced from the center of the Si_{28} cage. We calculated the influence of the variation in the position of the Na atom in this cage on the predicted Na charge and found significant differences (Table III). The charge ranged from a minimum of $0.646e^-$ at a displacement of 1 Å to a maximum of $0.865e^-$ at a displacement of 0.2 Å. XRD results show that displacement off-center may decrease with increasing Na content in Na_xSi_{136},[44] and the present calculations indicate that charge transfer would correspondingly increase with increasing x.

The Na in the smaller Si_{20} cage appears to reside in the center of the cage, and its calculated charge transfer is $0.681e^-$. Therefore, when the Na is closer on average to Si atoms, either due to being in the small Si_{20} cage or due to large displacement from the center of the large Si_{28} cage, the charge transfer is less than when the average Na-Si distance is longer.

C. Si *K*-edge EXAFS results

Figure 7 shows the normalized experimental Si K-edge XANES spectra [both fluorescent yield (FLY) and total-electron yield (TEY)] and EXAFS spectra (as TEY). In the XANES spectra presented in Fig. 7(a), an intense peak attributable to silicon oxide is observed in the TEY spectra and its intensity is significantly reduced in the FLY spectra. It has been established that TEY is more sensitive to the surface whereas FLY is more sensitive to the bulk.[48] Therefore, the XANES results indicate that the Si atoms on the surface of the samples were partially oxidized.

The edges of the Si spectra are redshifted relative to a crystalline Si wafer, indicating that the energy of the Si conduction-band minimum is lowered relative to the 1s core level and thus, a negative charge is borne by the Si framework. This is in keeping with previous studies[30] and with our finding of positive charge on the Na. However, the resolution of the present data was not sufficient to determine if charge transfer changed with varying Na content.

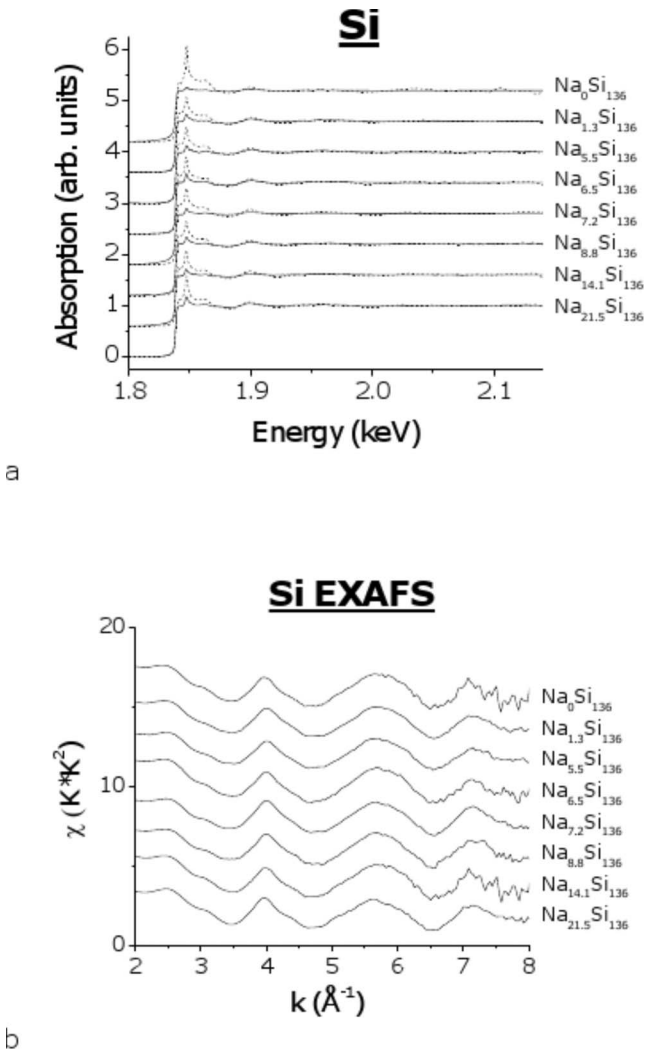

FIG. 7. Full Si K-edge experimental spectra for Na_xSi_{136}. (a) The XANES spectra for Na_xSi_{136}, where the dashed lines are the TEY signal which is sensitive to the surface, and the solid lines are FLY, which is sensitive to the bulk. The main observable difference is the varying intensity of the oxide peak at 1.849 keV. $Na_{x\to 0}Si_{136}$, prepared in 2003, and higher Na-content samples display more intense oxide peaks, as expected. (b) Si EXAFS observed for different concentration of Na in Na_xSi_{136}.

In the Si K-edge EXAFS spectra shown in Fig. 7(b), there is little difference with changing Na concentration throughout the entire spectral range. This consistency throughout the range of compositions is not surprising since Si dominates the composition of all samples and therefore most of the nearest neighbors to any absorbing atom were Si. Since the silicon concentration was essentially constant, the result was that no significant change in the nearest-neighbor interactions was observed with increasing Na content. This was supported by simulation of each unique Si position as well as in the combined weighted-average simulated spectra.

IV. CONCLUSIONS

The near-edge region of the x-ray absorption spectrum for a series of type II sodium-containing clathrates has been proven to be very sensitive to the local structure surrounding the absorbing Na atom. Relative cage occupation and off-center displacement were found to have profound effects on this region of the spectrum. However, due to the differences in cross sections of the two Na environments, it is only possible to use this information to indicate when the Si_{20} cages are nearly fully unoccupied. The EXAFS region on the other hand, by comparison to simulation, can be used to estimate the relative cage occupations when Na in the Si_{20} cages accounts for less than 30% of the overall Na content. The XAS data indicate that Na is preferentially lost from the Si_{20} cages, consistent with Rietveld analysis. Detailed EXAFS analysis for spectra from the highest Na content samples shows an increase in both displacement off-center of the Si_{28} cages and increased dynamic disorder with decreasing Na content. Calculated charge transfers were in qualitative agreement with observed edge shifts. Our systematic investigation of such a wide range of guest occupancies makes the present results serve as a useful reference for future studies of intermetallic clathrates.

ACKNOWLEDGMENTS

M.B. and G.S.N. acknowledge support from U.S. DOE under Grant No. DE-FG02-04ER46145 for sample synthesis, as well as powder XRD and analysis. M.B. acknowledges support from the University of South Florida. M.A.W. and P.Z. gratefully acknowledge support from NSERC. The Canadian Light Source (CLS) is supported by NSERC, CIHR, NRC, and the University of Saskatchewan. We acknowledge CLS staff scientists Robert Blyth and Tom Reiger (SGM beamline) for synchrotron technical support.

*Corresponding author; mary.anne.white@dal.ca

[1] J. S. Kasper, P. Hagenmuller, M. Pouchard, and C. Cros, Science **150**, 1713 (1965).
[2] G. S. Nolas, X. Lin, J. Martin, M. Beekman, and H. Wang, J. Electron. Mater. **38**, 1052 (2009).
[3] G. A. Slack, in *CRC Handbook on Thermoelectrics*, edited by D. M. Rowe (CRC Press, Boca Raton, FL, 1995).
[4] J. S. Tse and M. A. White, J. Phys. Chem. **92**, 5006 (1988).
[5] G. S. Nolas, G. A. Slack, and S. B. Schujman, Semicond. Semimetals **69**, 255 (2001).
[6] C. Uher, Semicond. Semimetals **69**, 139 (2001).
[7] Y. Liu, L. Wu, L. Li, S. Du, J. D. Corbett, and L. Chen, Angew. Chem., Int. Ed. **48**, 5305 (2009).
[8] D. Neiner, N. L. Okamoto, C. L. Condron, Q. M. Ramasse, P. Yu, N. D. Browning, and S. M. Kauzlarich, J. Am. Chem. Soc. **129**, 13857 (2007).
[9] S. B. Schujman, G. S. Nolas, R. A. Young, C. Lind, A. P. Wilkinson, G. A. Slack, R. Patschke, M. G. Kanatzidis, M. Ulutagay, and S.-J. Hwu, J. Appl. Phys. **87**, 1529 (2000).
[10] P. Rogl and D. M. Rowe, *Thermoelectrics Handbook: Macro to Nano* (CRC Press, Boca Raton, 2006).
[11] J. Kim, N. Okamoto, K. Kishida, K. Tanaka, and H. Inui, Acta Mater. **54**, 2057 (2006).
[12] S. Bobev and S. C. Sevov, J. Am. Chem. Soc. **123**, 3389 (2001).
[13] G. S. Nolas, T. J. R. Weakley, and J. L. Cohn, Chem. Mater. **11**, 2470 (1999).
[14] S. Bobev and C. Sevov, J. Solid State Chem. **153**, 92 (2000).
[15] J. S. Tse, K. Uehara, R. Rousseau, A. Ker, C. I. Ratcliffe, M. A. White, and G. MacKay, Phys. Rev. Lett. **85**, 114 (2000); **86**, 4980 (2001).
[16] G. S. Nolas, J.-M. Ward, J. Gryko, L. Qiu, and M. A. White, Phys. Rev. B **64**, 153201 (2001).
[17] L. Qiu, M. A. White, Z. Li, J. S. Tse, C. I. Ratcliffe, C. A. Tulk, J. Dong, and O. F. Sankey, Phys. Rev. B **64**, 024303 (2001).
[18] See, for example, L. Qiu, I. P. Swainson, G. S. Nolas, and M. A. White, Phys. Rev. B **70**, 035208 (2004).
[19] G. S. Nolas, T. J. R. Weakley, J. L. Cohn, and R. Sharma, Phys. Rev. B **61**, 3845 (2000).
[20] A. Ammar, C. Cros, M. Pouchard, N. Jaussaud, J. M. Bassat, G. Villeneuve, M. Duttine, M. Menetrier, and E. Reny, Solid State Sci. **6**, 393 (2004).
[21] J. Gryko, R. F. Marzke, G. A. Lamberton, Jr., T. M. Tritt, M. Beekman, and G. S. Nolas, Phys. Rev. B **71**, 115208 (2005).
[22] G. S. Nolas, M. Beekman, J. Gryko, G. A. Lamberton, Jr., T. M. Tritt, and P. F. McMillan, Appl. Phys. Lett. **82**, 910 (2003).
[23] N. J. English and J. S. Tse, Phys. Rev. Lett. **103**, 015901 (2009).
[24] M. Zakrzewski and M. A. White, Phys. Rev. B **45**, 2809 (1992).
[25] M. Beekman and G. S. Nolas, J. Mater. Chem. **18**, 842 (2008).
[26] E. Reny, P. Gravereau, C. Cros, and M. Pouchard, J. Mater. Chem. **8**, 2839 (1998).
[27] G. K. Ramachandran, J. Dong, J. Diefenbacher, J. Gryko, R. F. Marzke, O. F. Sankey, and P. F. McMillan, J. Solid State Chem. **145**, 716 (1999).
[28] S. B. Roy, K. E. Sim, and A. D. Caplin, Philos. Mag. B **65**, 1445 (1992).
[29] J. C. Conesa, C. Tablero, and P. Wahnon, J. Chem. Phys. **120**, 6142 (2004).
[30] É. Reny, M. Ménétrier, C. Cros, M. Pouchard, and J. Sénégas, C.R. Acad. Sci., Ser. IIc: Chim **1**, 129 (1998).
[31] J. He, D. D. Klug, K. Uehara, K. F. Preston, C. I. Ratcliffe, and J. S. Tse, J. Phys. Chem. B **105**, 3475 (2001).
[32] F. Tournus, B. Masenelli, P. Mélinon, D. Connétable, X. Blase, A. M. Flank, P. Lagarde, C. Cros, and M. Pouchard, Phys. Rev. B **69**, 035208 (2004).
[33] H. Libotte, J.-P. Gaspard, A. San Migueal, and P. Melinon, Europhys. Lett. **64**, 757 (2003).
[34] C. Cros, M. Pouchard, and P. Hagenmuller, J. Solid State Chem. **2**, 570 (1970).
[35] J. Gryko, P. F. McMillan, R. F. Marzke, G. K. Ramachandran, D. Patton, S. K. Deb, and O. F. Sankey, Phys. Rev. B **62**, R7707 (2000).
[36] A. C. Larson and R. B. Von Dreele, Los Alamos National Laboratory Report No. LAUR 86–748, 2004 (unpublished).
[37] B. H. Toby, J. Appl. Crystallogr. **34**, 210 (2001).

[38] L. D. Menard H. P. Xu, S. P. Gao, R. D. Twesten, A. S. Harper, Y. Song, G. L. Wang, A. D. Douglas, J. C. Yang, A. I. Frenkel, R. W. Murray, and R. G. Nuzzo, J. Phys. Chem. B **110**, 14564 (2006).

[39] A. L. Ankudinov, B. Ravel, J. J. Rehr, and S. D. Conradson, Phys. Rev. B **58**, 7565 (1998).

[40] See supplementary material at http://link.aps.org/supplemental/10.1103/PhysRevB.82.155207 for crystallographic data for all Na_xSi_{136} specimens from Rietveld refinement.

[41] M. Beekman, E. N. Nenghabi, K. Biswas, C. W. Myles, M. Baitinger, Y. Grin, and G. S. Nolas, Inorg. Chem. **49**, 5338 (2010).

[42] B. K. Teo, *EXAFS: Basic Principles and Data Analysis* (Springer-Verlag, New York, 1986).

[43] M. Beekman, W. Schnelle, H. Borrmann, M. Baitinger, Yu. Grin, and G. S. Nolas, Phys. Rev. Lett. **104**, 018301 (2010).

[44] M. Beekman, C. P. Sebastian, Yu. Grin, and G. S. Nolas, J. Electron. Mater. **38**, 1136 (2009).

[45] F. Brunet, P. Mélinon, A. San Miguel, P. Kéghélian, A. Perez, A. M. Flank, E. Reny, C. Cros, and M. Pouchard, Phys. Rev. B **61**, 16550 (2000).

[46] B. Wastberg, A. Rosen, and D. E. Ellis, Z. Phys. D: At., Mol. Clusters **13**, 153 (1989).

[47] M. Volmer, C. Sternemann, J. S. Tse, T. Buslaps, N. Hiraoka, C. L. Bull, J. Gryko, P. F. McMillan, M. Paulus, and M. Tolan, Phys. Rev. B **76**, 233104 (2007).

[48] P. Zhang, S. J. Naftel, and T. K. Sham, J. Appl. Phys. **90**, 2755 (2001).